© 2009 International Society of Nephrology

Imaging renal structures by X-ray phase-contrast microtomography

Jin Wu[1,2], Tohoru Takeda[1], Thet Thet Lwin[1], Atsushi Momose[3], Naoki Sunaguchi[4], Tadanori Fukami[4], Tetsuya Yuasa[4] and Takao Akatsuka[4]

[1]Institute of Clinical Medicine, Graduate School of Comprehensive Human Sciences, University of Tsukuba, Tsukuba-shi, Ibaraki, Japan; [2]Division of Clinical Neuroscience, Chiba University Center for Forensic Mental Health, Chiba, Japan; [3]Graduate School of Frontier Sciences, The University of Tokyo, Kashiwa, Chiba, Japan and [4]Graduate School of Science and Engineering, Yamagata University, Yonezawa, Yamagata, Japan

X-ray crystal interferometer–based X-ray phase-contrast microtomography (phase-contrast microtomography) is able to image microstructures within soft tissue without the use of a contrast agent. Here we determined the feasibility of using this technique in the non-destructive inspection of formalin-fixed kidney tissue from certain hamsters that spontaneously develop mesangial thickening with focal and segmental glomerulosclerosis, and from age-matched Syrian hamsters. We used a triple Laue-case X-ray interferometer with a 40 μm–thick analyzer, a sample cell, and an X-ray charge-coupled-device camera with a 4.34 μm pixel size. Images of glomeruli and tubular structures were similar to those seen using 40–100 × magnification on an optical microscope. In samples from two female glomerulosclerotic hamsters, seven scattered lesions were detected. The wedge-shaped pathological lesions included mild atrophic tubular walls, markedly dilated tubular lumen, high-density glomeruli, and widening of Bowman's space. The microvasculature was distinctly visualized in the specimens without any contrast agents. Hence, phase-contrast microtomography can detect small scattered lesions in diseased kidney tissue and is a powerful auxiliary tool for pre-histological evaluations.

Kidney International (2009) **75,** 945–951; doi:10.1038/ki.2009.42; published online 25 February 2009

KEYWORDS: APA hamster; biomedical imaging; glomerulus; renal microstructures; X-ray phase-contrast microtomography

Correspondence: *Tohoru Takeda, Institute of Clinical Medicine, Graduate School of Comprehensive Human Sciences, University of Tsukuba, Tsukuba-shi, Ibaraki 305-8575, Japan. E-mail: ttakeda@md.tsukuba.ac.jp*

Received 4 July 2008; revised 14 November 2008; accepted 7 January 2009; published online 25 February 2009

A small laboratory animal model of human diseases, such as the albino-panda-albino (APA) hamster, which is known to develop a spontaneous renal focal segmental glomerulosclerosis (FSGS) with age, has been used in the basic and premedical research of the kidney.[1,2] In a developed, spontaneous case of renal disease in the APA hamster, pathological findings, such as segmental sclerotic glomeruli, increased matrix, tubular atrophy, widening of Bowman's space, and thickening of the basement membrane, have been observed.[3,4] The detection of even a single glomerulus, involved with segmental sclerosis, is sufficient to invoke an initial diagnosis of FSGS. As the pathological diagnosis of FSGS with a scattered small pathological lesion is often missed, when only a few sliced sections are examined, a large enough sample, the sample site, and serial sliced sections are often required for exact diagnosis.

X-ray absorption-contrast micro-computer tomography at *ex vivo* state[5,6] and micro-magnetic resonance imaging at *in vivo* state[7] are used to image animals' kidney for biological researches. However, these techniques require contrast enhancement, and soft tissue composed of light elements cannot be well visualized. Recently, optical coherence tomography[8,9] and two-photon microscopy[10] have been reported for imaging *ex vivo* and/or *in vivo* kidney of small animals. The optical coherence tomography enables imaging of the high-resolution tomogram of 1–2 μm *in situ* and in real time; however, the observation depth is limited to 1–2 mm.[9] Two-photon microscopy can depict the distribution, behavior, and interactions of labeled chemical probes and proteins in live renal tissues at real time without fixation artifacts, and enables visualization with the depths of 150 μm.[10,11]

On the other hand, the X-ray phase-contrast imaging technique with a triple Laue-case crystal X-ray interferometer (Bonse–Hart type),[12] which has about a 1000-fold higher sensitivity for detecting the light element, such as hydrogen, carbon, nitrogen, and oxygen than the conventional X-ray absorption-contrast method, allows the visualization of biological soft tissues without needing a contrast agent.[13–15] Crystal X-ray interferometer-based X-ray phase-contrast tomography[16] successfully visualized fine morphological

structures of cancer lesions, such as cancerous mass, necrosis, fibrous capsule, fat tissue, and surrounding normal tissue in humans,[17] rabbits,[18] and mice.[19] Non-cancerous organs of rat and mouse, such as brain,[20] liver,[21] and heart were also visualized. In our earlier studies, phase-contrast tomography system with a spatial resolution of about 0.03 mm was used in a synchrotron radiation source at the Photon Factory of High Energy Accelerator Research Organization in Japan.[19] In the Photon Factory, the phase-contrast tomography system was developed to observe large objects of diameter 10–30 mm; therefore, the large crystal X-ray interferometer with a 1-mm thick analyzer[22] and its optimized X-ray camera[23] were manufactured. Thus, microstructures could not be visualized in detail.

To achieve a higher spatial resolution image of <0.01 mm, a crystal X-ray interferometer with a 40-μm thick analyzer was developed.[24,25] Using the X-ray phase-contrast microtomography system with this crystal X-ray interferometer (phase-contrast microtomography), we depicted the microstructure of kidney and spleen of rat earlier.[25,26] The purpose of this study is to examine the feasibility of phase-contrast microtomography for visualizing microstructures, and to analyze quantitatively the density alteration of microstructures in the kidney of APA hamsters.

RESULTS

In eight renal specimens from six hamsters (Table 1), two-dimensional (2D) and three-dimensional (3D) images were obtained using phase-contrast microtomography.

Imaging of renal microstructures

The phase-contrast microtomographic image discriminated clearly the microstructures of the renal cortex and medulla in normal kidney. The glomeruli, Bowman's space, various renal tubules, and vessels were well resolved (Figure 1).

The wedge-shaped pathological lesions including mild atrophic tubular walls, markedly dilated tubular lumens, glomeruli with high density, and widening of Bowman's space, were observed in renal specimens of two female APA hamsters (Figure 2). The size and localization of these pathological lesions were well visualized from the cortex to medulla using 3D imaging. These findings corresponded well to the histopathological picture (Figure 2f). However, the same findings were not detected in male APA hamsters, because the pathological change in them occurs much later compared with that in females.[1]

Wall thickness and lumen diameter of tubules were calculated in normal and abnormal areas of cortex (Figure 3). The thinnest tubular wall was about 12 μm. The glomerular volume was calculated and compared between the normal ($n=25$) and abnormal glomeruli ($n=17$) (Figure 4). The ratio of Bowman's space against glomerular volume in abnormal glomerulus was higher than those in normal glomerulus (Figure 4d). In addition, the mean density of glomerulus in pathological regions was higher than that in normal regions (Figure 4e). On measuring the density of normal glomerulus, percentile of abnormal glomerulus (normal mean density + 2 s.d.) was $\sim$57.7% in pathological regions in the APA hamster.

Imaging of renal microvasculature

The renal microvasculature was extracted from 3D phase-contrast microtomography images using the density threshold-based rendering technique. Distribution of the glomeruli, renal arteries, and veins were visualized successfully. Glomerular capillary tufts formed by capillary loop and surrounding tubules and vessels were observed clearly (Figure 5).

DISCUSSION

In this study, various microstructures and pathological changes of renal specimens in the APA hamster were observed at about 9.3 μm of spatial resolution. Glomeruli and tubular structures, were well depicted, and appeared similar to that of $\times$40–100 magnified optical microscopic image.

The APA hamsters are known to develop spontaneous FSGS with age[1,2] and mesangial thickening, in the renal glomeruli from an early stage.[2,3] Phase-contrast microtomography revealed mild atrophic tubular walls, markedly dilated tubular lumens, and widening of Bowman's space in renal specimens of females; these findings corresponded exactly to an earlier histopathological study.[4] Furthermore, phase-contrast microtomography enabled the assessment of the geometrical size and density of microstructures within the kidney; the thickness of abnormal tubules was about 42% thinner than that of normal tubules, and the density in abnormal glomeruli increased by about 2.6 mg/cm^3. The density resolution in this system is $\sim$1.2 mg/cm^3,[27] and the above-mentioned value is thought to be caused by the alteration of the renal glomerular matrix.

Usually, the diagnoses of abnormal renal microstructures and stage of FSGS progression are determined by optical microscopy, immunofluorescence, and electron microscopy.[4] In these methods, detection of a scattered lesion and a 3D spread of lesions are often difficult; therefore, (1) a large-enough sample must be used to detect the sclerotic glomeruli; (2) a serial sectional observation of the whole specimen is necessary for underestimating focal lesion; and (3) a huge number of sliced sections must be made and stained. However, these processes waste high costs and require large amounts of time for performance.

Recently, optical coherence tomography[8,9] and micro-magnetic resonance imaging[7] were applied to visualize renal microvasculature and microstructure non-destructively; however, a diagnostic study of FSGS has not yet been reported.

In X-ray absorption-contrast micro-computer tomography, the difference in density between blood and the surrounding soft tissue is very small; therefore, for visualizing the inner structures of kidney, it is essential to use a radio-opaque contrast agent including a heavy element.[5,6,28]

Table 1 | Summary of specimens

Specimen No.	Six	Age (months)	X-ray phase-contrast microtomographic finding: No. of focal abnormal lesions/samples	X-ray phase-contrast microtomographic finding: No. of widenings of Bowman's space
Normal				
1	Male	8	0/1	—
2	Female	8	0/1	
Abnormal				
3	Male	8	0/1	—
4	Male	8	0/1	—
5	Female	8	4/2	20/27 (74%)[a]
6	Female	8	3/2	17/22 (77%)[a]

[a]The detection rate of widening of Bowman's space of focal abnormal lesions in samples.

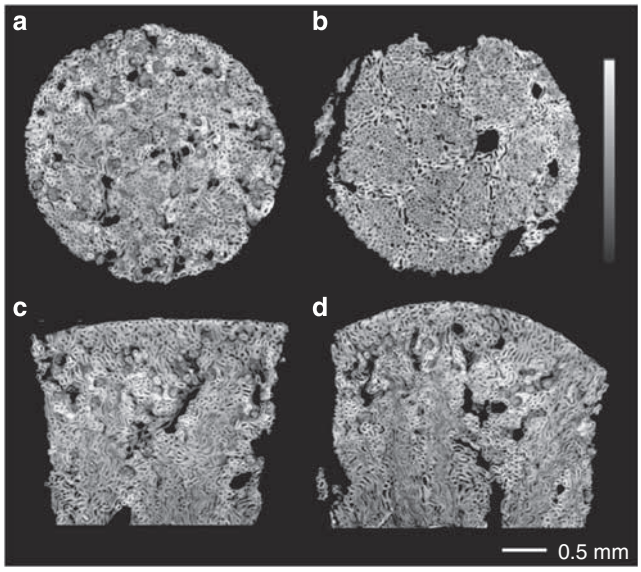

Figure 1 | X-ray phase-contrast microtomographic images of a normal hamster. (**a** and **b**) 2D images of axial, (**c**) coronal, (**d**) and sagittal view. (**a**) Glomeruli, vessels, and various tubules are depicted clearly in the renal cortex, (**b**) whereas in the renal medullary area, the collecting tube and its surrounding vessels are seen as lobule-like patterns. (**c** and **d**) Proximal and distal tubules are shown as high density, and the collecting tubules in the medullary area (including medullary ray) are shown as low density.

Microvasculature, such as the artery or vein can be imaged selectively by filling contrast agent in the target vessels; however, the surrounding soft tissue could not be visualized enough, due to low contrast among the significantly high-density contrast opacified vessels. In addition to homogeneously filling a vessel with contrast agent, a special preparation, such as pressure control injection is often required to infuse the contrast agent because of its high viscosity. These preparations might cause non-physiological conditions and artifacts, such as reactive constriction of the vessel and ischemia.

Four different types of the X-ray phase-contrast imaging techniques have been developed currently for biomedical research. Those are, crystal X-ray interferometer-based imaging,[16–18] diffraction enhanced imaging,[29–32] propagation-based imaging,[33,34] and grating X-ray interferometer-based imaging.[35,36] Propagation-based imaging is best for depicting edge information with large density differences. Diffraction enhanced imaging and grating X-ray interferometer-based imaging can detect much smaller density differences than propagation-based imaging. Diffraction enhanced imaging can clearly show breast cancer,[29] cartilage, and tendon.[30,31] Using the diffraction enhanced imaging technique, renal tubular structures of rat with 2- and 0.12-mm thick slices were visualized gently as projection image.[32] However, 3D renal microstructures have not yet been visualized tomographically, using these imaging techniques.

Crystal X-ray interferometer-based imaging is believed to have the highest sensitivity to observe the soft tissue structures in biomedical objects.[15] In fact, phase-contrast microtomography, without a specific preparation of samples, enables us to visualize fine 2D and 3D renal micro-architectures of kidneys, and to analyze quantitatively.

In this experiment, blood was washed out from renal vessels to eliminate artifact, because the coagulated blood in a vessel can be depicted in an X-ray phase-contrast image,[37] and as the different states of coagulation causes varying image contrast. After injection of physiological saline, the hepatic vessel of rat could be visualized clearly by X-ray phase-contrast radiography, whereas the X-ray absorption-contrast image could not depict the vessel at the same X-ray dose and energy.[21] Therefore, renal perfusion was carried out using physiological sodium solution for separating the vessel. This procedure was much easier and is thought to preserve more physiological conditions than the usage of conventional contrast agents with high viscosity. The fine density difference among physiological saline within tubules, vessels, and the surrounding soft tissue of kidney, was discriminated sufficiently on the images. In addition, using a volume-rendering technique, the renal microstructures and microvasculature could be depicted from the same specimen at by one scan.

Thus, phase-contrast microtomography might be used as a powerful auxiliary tool for a pre-histological evaluation of the APA renal disease model for detecting small scattering lesions and their spread.

In the present limitation of this system, the field of view was only 5×5 mm, because of the size of the X-ray beam and X-ray charge coupled device camera (see Figure 6). For phase-contrast microtomography, we need the synchrotron radiation with advantageous properties, such as high photon flux density, energy tunability, and natural collimation. To use such a system on the desktop, special high flux X-ray source must be developed newly.

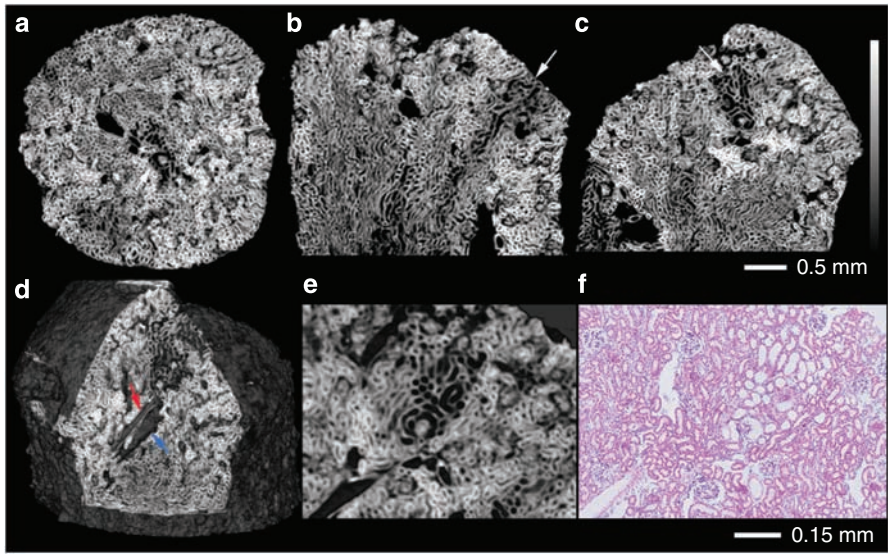

Figure 2 | X-ray phase-contrast microtomographic images of a female APA hamster. (**a**–**c**) 2D images of axial, coronal, and sagittal views, (**d**) 3D image, (**e** and **f**) magnified image of renal cortex corresponding to an image using a light microscope. Wedge-shaped lesions including markedly dilated tubule and widening of Bowman's space are shown (white arrow). (**e**) Phase-contrast microtomography shows the resemblance to (**f**) a light microscopic image. Red arrow, renal artery; blue arrow, renal vein.

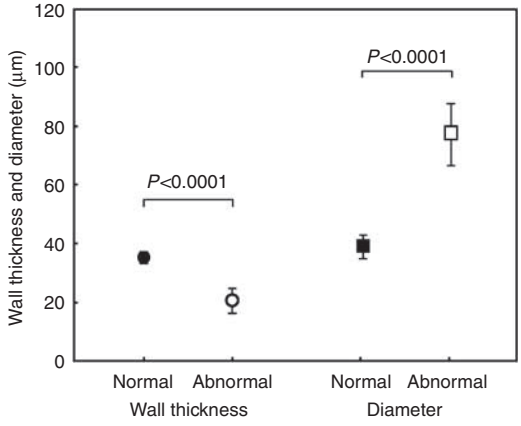

Figure 3 | Wall thickness and lumen diameter of tubules in normal and abnormal area of cortex. Thin tubular walls and dilated lumens are observed in abnormal areas of the cortex. The mean wall thickness of tubules in the cortex is 35.3 ± 2.1 and $20.4 \pm 4.3\,\mu m$ ($P < 0.0001$) in normal and abnormal area, respectively; the thickness of abnormal tubule is about 42% thinner than that of normal tubule. Mean diameter of tubular lumen was 40.0 ± 4.1 and $77.1 \pm 10.5\,\mu m$ ($P < 0.0001$) in normal and abnormal areas of the cortex. Of 49 glomeruli in 7 focal abnormal lesions, the widening of Bowman's space was observed in 37 glomeruli (75.5%).

MATERIALS AND METHODS

Preparation of animals

Six small animals including four APA hamsters (8 months, two females and two males) and two age-matched normal hamsters (1 female and 1 male) were used in our experiments (Table 1). All subjects were anesthetized by an i.p. injection of sodium pentobarbital (50 mg/kg body weight), and cannulation to the apex of left ventricle was carried out surgically. The physiological saline solution was injected from the apex, and the whole blood was replaced to eliminate artifacts of blood coagulation within the vessel. The kidneys were extracted quickly and fixed using 10% formalin. These kidneys were then cut into column specimens of 3-mm diameter for a computed tomography observation, because the field of view was limited to 5×5 mm. A total of eight samples were imaged.

This experiment was approved by the Medical Committee for the Use of Animals in Research of the University of Tsukuba, and it conformed to the guidelines of the American Physiological Society.

X-ray phase-contrast microtomographic system

The phase-contrast microtomographic system[24,25] (Figure 6) consists of a triple Laue-case crystal X-ray interferometer (Bonse–Hart type) with a 40-μm thick analyzer,[25] a phase shifter, a target sample cell, and an X-ray charge coupled device camera of pixel size $4.34 \times 4.34\,\mu m$. The interferometer with a 40-μm thick analyzer was manufactured to obtain a high spatial resolution of < 0.01 mm by decreasing burring of the image caused by diffraction in the analyzer. The reconstructed voxel size of phase-contrast microtomogram is $4.34 \times 4.34 \times 4.34\,\mu m^3$. Experiments were carried out at the undulator beam-line 20XU (SPring-8, Japan).

The spatial resolution in this system was estimated from the observed point spread function at the edge of pathological object and surrounding formalin solution, and was about 9.3 μm. The density resolution was $\sim 1.2\,mg/cm^3$.[27]

Data acquisition and image reconstruction

In phase-contrast microtomography, a specimen was placed in a 5-mm thick sample cell filled with formalin, and this cell was inserted in the beam path of the interferometer. The X-ray energy was set at 12.4 keV. The beam exposure time was 5 s/projection and the number of projections was 250 over 180°. Details of the image reconstruction process, namely, fringe-scan data acquisition technique and image reconstruction methods, have been earlier described.[16] The parameters of data acquisition are shown in Table 2.

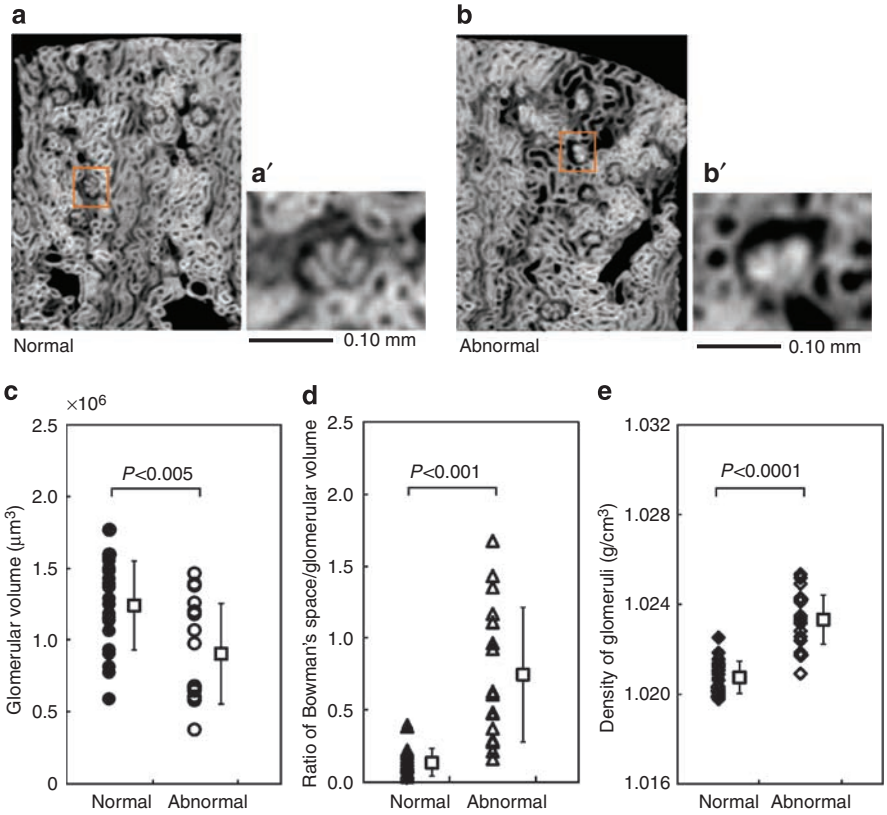

Figure 4 | Quantitative analysis of glomerulus images obtained by X-ray phase-contrast microtomography. (**a** and **b**) X-ray phase-contrast microtomographic images of normal and abnormal area and (**a′** and **b′**) magnified images of glomerular images from panels a and b; (**c**–**e**) glomerular volume, ratio of Bowman's space, and density between the normal and abnormal glomerulus. (**c**) The mean volume is $(1.24 \pm 0.31) \times 10^6\ \mu m^3$ and $(0.91 \pm 0.35) \times 10^6\ \mu m^3$ in normal and abnormal glomeruli, respectively ($P < 0.005$). (**d**) The ratio of Bowman's space against glomerular volume of abnormal glomeruli is higher than those of normal glomeruli (0.74 ± 0.47 vs 0.13 ± 0.10, $P < 0.001$). (**e**) Density of abnormal glomerulus is about 2.6 mg/cm^3 higher than that of normal glomerulus (1023.3 ± 1.1 vs 1020.7 ± 0.7 mg/cm^3, $P < 0.0001$).

Quantitative analysis

3D imaging display. Phase-contrast microtomograms were analyzed using the real-time 3D volume-rendering software (Real INTAGE; KGT Inc., Japan) on a workstation (Precision; Dell, Round Rock, TX, USA). This software provides several integrated tools for 3D image data management, such as density measurement, data processing, and 3D display. The volume-rendering tool, especially, is quite convenient to present the 3D architecture of renal vasculature. By interactive selection of processing parameters, we can depict the microstructures and the microvasculature of specimens and glomeruli. Thus, we enabled to generate 2D and 3D microstructures and the microvasculature of specimens, and glomeruli images. Multiplanar reformatting techniques allowed us to view the data set in transverse, sagittal, coronal, and even the sectional planes of any angle.

Volume analysis. Each volume of glomerulus and Bowman's space was calculated using image-processing software. First, the cutoff threshold of glomerulus was decided from the images of 25 normal glomeruli. Using this threshold, each glomerulus and outer Bowman's space was margined automatically. However, the margin of glomerulus and the outer Bowman's space attached to the surrounding tissues were determined manually. Then, we extracted the glomerulus itself and the surrounding Bowman's space using the image binarization technique. Finally, the number of pixels in each area was counted in each slice, and its volume was calculated in 3D images.

Density analysis. We can determine the refraction index directly from phase shift information. The mass density at glomerulus was calculated approximately by the equation:

$$\frac{\delta_s}{\delta_w} \times 1g/cm^3$$

in which, δs and δw are refraction index decrements from unity of glomerulus and surrounding 10% formalin solution, respectively. The δw is 1.5024×10^{-6} at 12.4 keV X-ray energy. The parameter, δs, is measured as an average value of each glomerular region on phase-contrast microtomogram.

To estimate the 3D density of each glomerulus, the margin of glomerulus was picked up interactively on the image processing workstation, and the refractive index of glomerulus was first measured on each trans-axial image. The density in 3D space was calculated by integrating the refractive index on each trans-axial image from the upper pole to lower pole of the glomerulus.

Histophathological analysis

After phase-contrast microtomography imaging, all specimens were sliced into 3-μm thick sections, and then hematoxylin-eosin staining

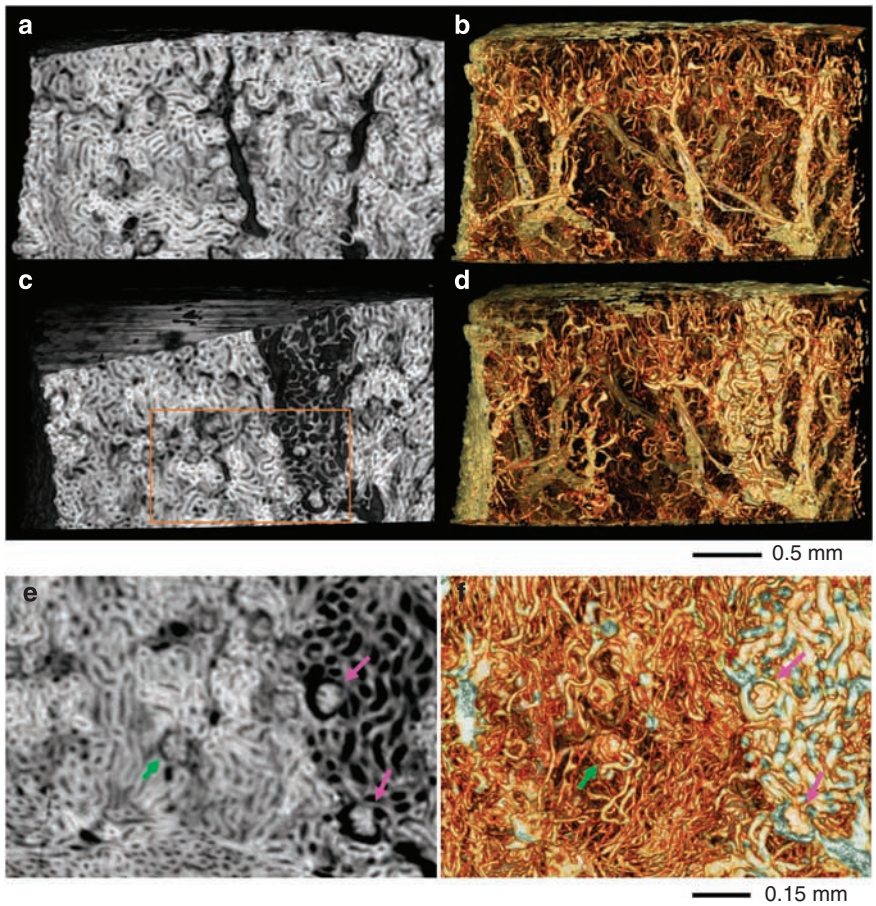

Figure 5 | Image of renal microstructure and vasculature obtained by X-ray phase contrast microtomography. (**a** and **c**) X-ray phase-contrast microtomogram of renal cortex and (**b** and **d**) three-dimensional extracted renal microvasculature and tubule of normal and abnormal area in an APA hamster. (**e** and **f**) The magnified images are from the rectangular area in Figure 1c. Distribution of the renal arteries and veins was visualized successfully. The capillary tufts are observed clearly in normal glomerulus (green arrows), whereas the widening of Bowman's space and the indistinct pattern of the capillary loop are observed in abnormal glomerulus (pink arrows). In the three-dimensional image, non-dilated tubules and non-atrophic glomeruli are shown in normal cortical areas, whereas dilated tubules and atrophic glomeruli are depicted clearly in the FSGS lesions.

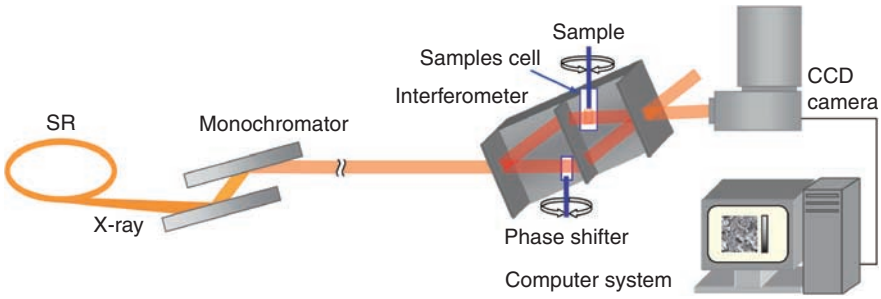

Figure 6 | Experimental setup for the X-ray phase-contrast microtomography. This system[25] consists of a Bonse–Hart type of crystal X-ray interferometer, a phase shifter, a sample cell, and an X-ray CCD camera with a pixel size of 4.34 × 4.34 μm. The interferometer with a 40 μm–thick analyzer was manufactured to obtain the spatial resolution of about 0.01 mm. The estimated spatial resolution is 9.3 μm. CCD, charge-coupled device; SR, synchrotron radiation.

Table 2 | Parameters of data acquisition

Field of view	X-ray energy	Sample detector distance	Pixel size of X-ray CCD camera (number of pixels)	Exposure time	Number of projections
5 × 5 mm	12.4 keV	~10 cm	4.34 × 4.34 μm (1344 × 1024)	5 s /projection	250/180°

CCD, charge-coupled device.

and periodic acid-Schiff staining were carried out to examine the histopathological structures. Histopathological images were assessed using an optical microscope equipped with a camera (Biozero; KEYENCE Co., Japan).

Statistical analysis

All data were expressed as mean ± s.d.. The differences between groups were analyzed using Student's unpaired *t*-test. $P<0.05$ was considered statistically significant.

DISCLOSURE

All the authors declared no competing interest.

ACKNOWLEDGMENTS

This research was supported by a Special Coordination Fund and Grant-in-Aid for Scientific Research in Priority Areas (#17591244, #17659362, #19659302) from the Ministry of Education, Culture, Sports, Science and Technology of the Japanese government, and was carried out under the approval (2004B0426-NL-np) of the committee of SPring-8, Japan. The authors thank Mr Yoshitaka Hamaishi for the LLL interferometer; Mr Ichirou Koyama, Ms Akiko Fujii (The University of Tokyo), and Mr Yoshio Suzuki (SPring-8) for technical support; Mr Toshihiko Kimura and Mr Hideo Kahara (KGT Inc.) for technical support of software; Mr Kouzou Kobayashi for preparation of experimental apparatus, and Ms Yukiko Kawata for the preparation of this paper.

REFERENCES

1. Doi K, Yamamoto T, Isegawa N *et al.* Age-related non-neoplastic lesions in the heart and kidneys of Syrian hamsters of the APA strain. *Lab Anim* 1987; **21**: 241–248.
2. Nishida E, Yamanouchi J, Ogata S *et al.* Age-related histochemical and ultrastructural changes in renal glomerular mesangium of APA hamsters. *Exp Anim* 1996; **45**: 339–345.
3. Han JS, Norimatsu M, Itagaki S *et al.* Early development of spontaneous glomerular lesion in Syrian hamsters of APA strain. *J Vet Med Sci* 1992; **54**: 149–151.
4. Inenaga T, Nishida E, Kawamura S *et al.* Renal function tests on diabetes-induced and non-induced APA hamsters. *Exp Anim* 2002; **51**: 437–445.
5. Ortiz MC, Garcia-Sanz A, Bentley MD *et al.* Microcomputed tomography of kidneys following chronic bile duct ligation. *Kidney Int* 2000; **58**: 1632–1640.
6. Fortepiani LA, Ruiz MCO, Passardi F *et al.* The effect of losartan on renal microvasculature during chronic inhibition of nitric oxide visualized by micro-CT. *Am J Physiol Renal Physiol* 2003; **285**: 852–860.
7. Kobayashi H, Kawamoto S, Jo SK *et al.* Renal tubular damage detected by dynamic micro-MRI with a dendrimer-based magnetic resonance contrast agent. *Kidney Int* 2002; **61**: 1980–1985.
8. Chen Y, Andrews PM, Aguirre AD *et al.* High-resolution three-dimensional optical coherence tomography imaging of kidney microanatomy ex vivo. *J Biomed Opt* 2007; **12**: 034008.
9. Andrews PM, Chen Y, Onozato ML *et al.* High-resolution optical coherence tomography imaging of the living kidney. *Lab Invest* 2008; **88**: 441–449.
10. Ashworth SL, Sandoval RM, Tanner GA *et al.* Two-photon microscopy: visualization of kidney dynamics. *Kidney Int* 2007; **72**: 416–421.
11. Russo LM, Sandoval RM, McKee M *et al.* The normal kidney filters nephrotic levels of albumin retrieved by proximal tubule cells: retrieval is disrupted in nephrotic states. *Kidney Int* 2007; **71**: 504–513.
12. Bonse U, Hart M. An X-ray interferometer. *Appl Phys Lett* 1965; **6**: 155–156.
13. Momose A, Fukuda J. Phase-contrast radiographs of nonstained rat cerebellar specimen. *Med Phys* 1955; **22**: 375–379.
14. Takeda T, Momose A, Itai Y *et al.* Phase-contrast imaging with synchrotron X-rays for detecting cancer lesions. *Acad Radiol* 1995; **2**: 799–803.
15. Fitzgerald R. Phase-sensitive X-ray imaging; new approaches that can detect X-ray phase shifts within soft tissues show promise for clinical and biological applications. *Phys Today* 2000; **53**: 23–28.
16. Momose A. Demonstration of phase-contrast X-ray computed tomography using an X-ray interferometer. *Nucl Instrum Methods Phys Res* 1995; **A352**: 622–628.
17. Takeda T, Momose A, Hirano K *et al.* Human carcinoma: early experience with phase-contrast X-ray CT with synchrotron radiation-comparative specimen study with optical microscopy. *Radiology* 2000; **214**: 298–301.
18. Momose A, Takeda T, Itai Y *et al.* Phase-contrast X-ray computed tomography for observing biological soft tissue. *Nat Med* 1996; **2**: 473–475.
19. Takeda T, Wu J, Lwin TT *et al.* Interferometer-based phase-contrast X-ray CT of colon cancer specimens: comparative study with 4.74 tesla MRI and optical microscopy. *J Comput Assist Tomogr* 2007; **31**: 214–217.
20. Beckmann F, Heise K, Kolsch B *et al.* Three-dimensional imaging of nerve tissue by X-ray phase-contrast microtomography. *Biophys J* 1999; **76**: 98–102.
21. Takeda T, Momose A, Wu J *et al.* Vessel imaging by interferometric phase-contrast x-ray technique. *Circulation* 2002; **105**: 1708–1712.
22. Takeda T, Momose A, Yu Q *et al.* Phase-contrast x-ray imaging with a large monolithic x-ray interferometer. *J Synchrotron Radiat* 2000; **7**: 280–282.
23. Momose A, Takeda T, Yoneyama A *et al.* Wide-area phase-contrast X-ray imaging using large X-ray interferometers. *Nucl Instrum Methods Phys Res* 2001; **A467-468**: 917–920.
24. Momose A, Koyama I, Hirano K. Improvement of spatial resolution in phase-contrast X-ray computed tomography. *Proc Soc Photo Opt Instrum Eng* 2001; **4503**: 71–81.
25. Momose A, Koyama I, Hamaishi Y *et al.* Phase-contrast microtomography using an X-ray interferometer having a 40-μm analyzer. *J Phys* 2003; **104**: 599–602.
26. Wu J, Takeda T, Lwin TT *et al.* Micro-phase-contrast X-ray computed tomography for basic biomedical study in SPring-8. *Proc Soc Photo Opt Instrum Eng* 2004; **5535**: 740–747.
27. Momose A. Phase-sensitive imaging and phase tomography using X-ray interferometers. *Opt Express* 2003; **11**: 2303–2314.
28. Toyota E, Ogasawara Y, Fujimoto K *et al.* Global heterogeneity of glomerular volume distribution in early diabetic nephropathy. *Kidney Int* 2004; **66**: 855–861.
29. Rocha HS, Pereira GR, Faria P *et al.* Diffraction-enhanced imaging microradiography applied in breast samples. *Eur J Radiol* 2008; **68S**: S37–S40.
30. Koyama I, Momose A, Wu J *et al.* Biological imaging by X-ray phase tomography using diffraction-enhanced imaging. *Jpn J Appl Phys* 2005; **44**: 8219–8221.
31. Muehleman C, Li J, Zhong Z *et al.* Multiple-image radiography for human soft tissue. *J Anat* 2006; **208**: 115–124.
32. Li G, Chen Z, Wu Z *et al.* Image quality dependence on thickness of sliced rat kidney taken by a simplest DEI construction. *Nucl Instrum Methods Phys Res* 2005; **A548**: 200–206.
33. Snigirev A, Snigireva I, Kohn V *et al.* Phase contrast microimaging by coherent high energy synchrotron radiation. *Rev Sci Instrum* 1995; **66**: 5486–5492.
34. Cloetens P, Ludwig W, Baruchel J *et al.* Holotomography: quantitative phase tomography with micrometer resolution using hard synchrotron radiation x-rays. *Appl Phys Lett* 1999; **75**: 2912–2914.
35. Weitkamp T, Diaz A, David C. X-ray phase imaging with a grating interferometer. *Opt Express* 2005; **13**: 6296–6304.
36. Betz O, Wegst U, Weide D *et al.* Imaging applications of synchrotron X-ray phase-contrast microtomography in biological morphology and biomaterials science. I. General aspects of the technique and its advantages in the analysis of millimetre-sized arthropod structure. *J Microsc* 2007; **227**: 51–71.
37. Momose A, Takeda T, Itai Y. Blood vessels: depiction at phase-contrast x-ray imaging without contrast agents in the mouse and rat – feasibility study. *Radiology* 2000; **217**: 593–596.